Journal of Marine Science and Application (2026) 25: 444-457
https://doi.org/10.1007/s11804-026-00911-9

RESEARCH ARTICLE

Assessing the Influence of Operational and Geometric Parameters on the Hydrodynamic Performance of Vertical-axis Marine Current Turbines

Minh Thao Nguyen[1], Francesco Balduzzi[2], Alessandro Bianchini[2] and Anders Goude[1]

Received: 04 November 2025 / Accepted: 01 March 2026

Abstract

The hydrodynamic behavior of vertical-axis marine current turbines is analyzed through a multivariate study considering various combinations of blade numbers, chord lengths, and rotor radii across 16 geometrical configurations operating over a wide range of tip speed ratios (TSRs) using two-dimensional computational fluid dynamics (CFD) simulations. The results reveal that reducing the number of blades from 6 to 3 at a given solidity can increase the power coefficient by up to 7.9%. However, this performance gain comes at the cost of a considerable increase in torque fluctuation amplitude, which in water applications could affect structural loading and operational stability. While these results align well with the literature in aggregate, the present study provides additional insights by reconstructing lift and drag polars using an advanced methodology to extract the instantaneous angle of attack of the flow approaching the blades. This approach provides not only a more in-depth analysis of blade hydrodynamics under unsteady conditions but also contextualizes the impact of the Reynolds number and chord-to-radius (c/R) ratio on turbine performance through the virtual cambering effect. The results demonstrate that higher Reynolds numbers enhance resistance to flow separation, while larger chord lengths amplify the virtual curvature effect. These findings improve the understanding of the interplay between key geometric and operational parameters, offering valuable guidance for optimizing vertical-axis turbine design in marine energy applications.A simple local watertight plate adjustment in the high-risk area can improve the safety of the ship.

Keywords Vertical-axis turbine; Hydrokinetic turbine; Design; Unsteady aerodynamics

1 Introduction

One of the major challenges facing mankind today is climate change, and the goal is to achieve net-zero carbon emissions by mid-century (Allan et al., 2021; Allan et al., 2019). These challenges can be overcome by employing a full suite of renewable technologies. In the electricity sector, renewable energy technologies are key to reducing emissions, currently the single largest source of CO_2 emissions (International Energy Agency (IEA), 2022). Electricity is the most widely used form of energy consumption, making it essential for all renewable energy forms, including wind, solar, and marine currents, to continue expanding and become integral parts of the energy mix (Kamani and Ardehali, 2023). The primary energy supply mix will change considerably over the next 30 years (Gielen et al., 2019). with the fossil share falling from 80% to just below 50% by 2050 (OECD, 2012). The nuclear energy share is expected to remain stable at 5% over the entire period, while the renewable share is forecast to triple from 15% to 45% by the end of the projection period (DNV, 2021). In the pathway to net zero, almost 90% of global electricity generation in 2050 will come from renewable sources (Newell et al., 2019).

The potential global market for marine current power ranges between 150 and 800 TWh per year, or up to EUR 40 billion per year. Under favorable regulatory and economic conditions, ocean energy technologies (marine current and wave) could potentially fulfill 10% of the EU's power demand by 2050 (Bachant and Wosnik, 2016; Rainbird et al., 2015; Melikoglu, 2018). The growing need for ocean energy makes the study of marine current energy

Article Highlights

- Reducing the blade number from 6 to 3 increases the maximum power coefficient by 7.9%.
- Transitioning from 3 to 4 blades drastically reduces torque fluctuations.
- Larger chord-to-radius ratios amplify the virtual curvature effect on the blades.
- Commercial-scale turbine configurations exhibit Reynolds-independent performance behavior.

✉ Minh Thao Nguyen
minh-thao.nguyen@angstrom.uu.se

[1] Department of Electrical Engineering, Uppsala University, Uppsala 75103, Sweden

[2] Department of Industrial Engineering, University of Florence, Florence 50139, Italy

converters an active research topic. Many device developers are currently working at prototype and demonstration stages to build fairly large pre-commercial turbines (e.g., the 1.2 MW SeaGen and 2 MW OpenHydro devices) (Zhou et al., 2017).

Marine current energy is typically harvested using two types of turbines classified by their rotational axis: horizontal-axis turbines (HATs) and vertical-axis turbines (VATs). While still industrially underdeveloped compared with their horizontal-axis counterparts, VATs can theoretically offer some advantages over HATs. First, VATs capture flow from any direction, eliminating the need for active yaw systems, making them well-suited for areas with variable or turbulent currents. Second, their simpler architecture, which allows the generator to be easily accessible outside the area swept by the blades, can reduce maintenance costs and improve long-term reliability. These advantages have driven considerable research interest in VATs. However, their development presents challenges owing to complex unsteady flow dynamics and operational characteristics (Li et al., 2023). Several studies have examined key VAT design parameters such as solidity (number of blades, chord length, turbine diameter) (Zhu et al., 2019; Subramanian et al., 2017), blade profile and hydrofoil (Subramanian et al., 2017; Shukla and Kaviti, 2017; Rainbird et al., 2015; Ismail and Vijayaraghavan, 2015; Hand et al., 2017; Jafari et al., 2018), rotor profile parameters (blade installation angle, height-to-diameter ratio) (Zamani et al., 2016a; Zamani et al., 2016b; Divakaran et al., 2021), and Reynolds number (Bachant and Wosnik, 2016; Hand et al., 2017; Zanforlin and Deluca, 2018; McTavish et al., 2013). Most of these studies, however, focused on vertical-axis wind turbines, which share the same operating principle as marine current turbines but may have different requirements owing to the differences that fluids with markedly different density and viscosity can induce in unsteady fluid-dynamic effects. Table 1 summarizes the key geometrical and operational parameters studied in the literature along with the primary research objectives. The primary focus areas include the effects of solidity (or number of blades), Reynolds number, and blade profile or chord length.

As is well established, solidity is often considered one of the key design parameters in VATs, as it drives efficiency (the more permeable the turbine is to the incoming flow, i. e., with low solidity, the higher is the theoretical efficiency) but also the optimal tip speed ratio (TSR) (lower solidity requires higher TSRs); moreover, solidity quantifies the impact of the flow curvature effect on airfoil/hydrofoil performance (Rainbird et al., 2015). However, solidity alone cannot provide an exhaustive overview of the interplay among the various design variables. In this regard, the studies in Table 1 sometimes led to contradictory results. For example, most studies that investigate the effect of blade number tend to keep the chord length and the turbine radius constant; this, in turn, means that solidity changes, and thus its impact on performance is superimposed on that of blade number alone. From this perspective, turbines with different solidities should be treated as distinct designs rather than variations of the same turbine. To isolate the effects of other parameters, solidity should be kept constant. Another limitation of most studies presented to date was the low range of chord-based Reynolds numbers, typically below 5×10^5. Experiments are often conducted in controlled environments such as water tanks, wind tunnels, or laboratories, necessitating the use of small-scale turbines. Consequently, there is a notable lack of experimental and numerical data for higher Reynolds numbers representative of hydrokinetic or commercial-scale turbines.

These research gaps motivate the present study, which aims to comprehensively investigate the effects of key design parameters on hydrokinetic vertical-axis turbine performance. This study contributes to the literature in the following ways:

- Solidity is kept constant when evaluating the impact of

Table 1 Literature survey

Objective effect	Number of blades, N	Radius, R (m)	Chord, c (m)	TSR	Re_c ($\times 10^5$)	Validation turbine
Solidity	2, 3, 4 (Rezaeiha et al., 2018)	0.5	0.025–0.18	1.5–5.5	0.51–6.41	2- and 3-blade
	2, 3, 4 (Subramanianet al., 2017)	1.35	0.42	1–2.5	–	3-blade
	2, 3, 4 (Sagharichi et al., 2018)	1	0.03–0.1	0.5–3.5	–	3-blade
	2, 3, 4, 5 (Li et al., 2016)	1	0.26	0.5–3.0	1.85–2.89	2-, 3-, 4-, 5-blade
	2, 3, 4, 5, 6 (Zhu et al., 2019)	0.5	0.06, 0.08	1.4–3.4	–	3-blade
	2, 3, 4, 5 (Miller et al., 2021)	0.048	0.0216	0.8–2.0	2.0–47	
Reynolds number	3 (Bachant and Wosnik, 2016)	0.5	0.14	0.5–3.4	0.5–3.5 (2.0)	3-blade
	3 (Leonardo et al., 2012)	0.064	–	3.5–6.0	0.1–1.73* (4.0)	3-blade horizontal
	2 (Walker et al., 2014)	0.4	–	5–11	(5.0)	2-blade horizontal water
Blade profile/ chord	3 (Ma et al., 2018)	0.4	0.2	0.4–1.5	–	
	3 (Tong et al., 2023)	0.3 – 4.0	0.05–0.8	0.2–4.8	–	2- and 3-blade

Note: "*": The range of Reynolds number is calculated based on the rotor diameter, while the independent Reynolds number is estimated by the chord length

individual parameters, allowing for a fairer isolation of each parameter's effects compared with other studies.

• The study analyzes the combined impact of geometrical and operational parameters across ranges representative of hydrokinetic turbines. Geometrical parameters include the number of blades, blade-chord length, and turbine radius, while operational parameters vary across a wide range of TSRs (2.0–4.5) and chord-based Reynolds numbers from 3.0×10^5 to 5×10^6, which are of direct interest for medium-scale commercial turbines. This enables an accounting of the complex interplay among the parameters, such as the impact of flow curvature effects, and especially virtual camber. Experimental validation for a similar machine is also provided.

• The contributions of dynamic lift and drag forces to dynamic blade loading are investigated to provide deeper hydrodynamic insights. This analysis clarifies how geometrical and operational parameters collectively influence performance.

The study is organized as follows. Section 2 presents the case study and the test matrix, while Section 3 describes the numerical CFD model. The results are discussed in Section 4. Finally, Section 5 highlights the major outcomes of the study.

2 Case study

2.1 Objective of the current work

To analyze the impact of variations in geometrical and operational parameters on hydrokinetic turbine performance, three values of global turbine solidity (σ) are considered: 0.102, 0.153, and 0.204. These values lie in the range identified in the existing literature as the most promising for VATs. For each solidity value, other parameters are systematically varied, including blade number, chord length, turbine radius, TSR, and Reynolds number. Specifically, the blade number ranges from 3 to 6, the chord length spans 13 different values from 0.1 m to 0.8 m, and the turbine radius is set to either 2.94 m or 5.88 m. The TSR varies within a broad range from 2.0 to 4.5, and the blade-chord Reynolds number spans from 2.8×10^5 to 5.0×10^6. As a result, 16 distinct turbine configurations are examined, with details provided in Table 2.

2.2 Performance parameters

Figure 1 shows the top view of a counter-clockwise rotating blade, where the reference system, force, and velocity vectors are represented for azimuthal position θ. In the following equations, the design variables are reported as height, H (m); radius, R (m); chord length, c (m); number of blades, N; blade solidity, σ; water velocity, v (m/s); and relative velocity, V_{rel} (m/s).

Table 2 Dimensions of the turbine and blade parameters across 16 study cases

N	σ	c/R	c (m)	R (m)	Re_c ($\times 10^5$)	TSR
3-blade	0.102	0.0680	0.200	2.94	5.5–12.5	2.0–4.5
	0.153	0.1020	0.300	2.94	8.3–18.8	
	0.204	0.1360	0.400	2.94	11.1–25.0	
	0.204	0.1360	0.800	5.88	22.2–50.0	
4-blade	0.102	0.0510	0.150	2.94	4.2–9.4	
	0.153	0.0765	0.225	2.94	6.3–14.1	
	0.204	0.1020	0.300	2.94	8.4–18.8	
	0.204	0.1020	0.600	5.88	16.8–37.6	
5-blade	0.102	0.0408	0.120	2.94	3.3–7.5	
	0.153	0.0612	0.180	2.94	5.0–11.3	
	0.204	0.0816	0.240	2.94	6.7–15.0	
	0.204	0.0816	0.480	5.88	13.4–30.0	
6-blade	0.102	0.0340	0.100	2.94	2.8–6.3	
	0.153	0.0510	0.150	2.94	4.2–9.4	
	0.204	0.0680	0.200	2.94	5.6–12.5	
	0.204	0.0680	0.400	5.88	11.2–25.0	

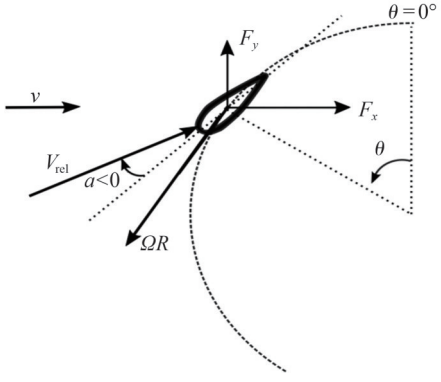

Figure 1 Blade rotating coordinate system, hydrodynamic forces and symbol conventions

Two critical parameters that govern the flow conditions experienced by the airfoil and its intrinsic aerodynamic efficiency, respectively, are the TSR(λ) and the chord-based Reynolds number (Re_c). These parameters are defined by Equations (1) and (2), respectively:

$$\lambda = \frac{\Omega R}{V} \tag{1}$$

$$Re_c = \frac{\rho \Omega R c}{\mu} \tag{2}$$

As discussed, a key parameter for characterizing both VAT geometry and its interaction with the flow is the solidity (σ), which incorporates the contributions of the number of blades, chord length, and turbine diameter as expressed in Equation (3).

$$\sigma = \frac{Nc}{2R} \tag{3}$$

Turbine loads in the study are modeled via the axial thrust coefficient (Equation (4)) and the torque coefficient (Equation (5)):

$$C_{X,(Y)} = \frac{\frac{1}{2\pi}\int_{\theta}^{\theta+2\pi}\sum_{i=1}^{N} F_{X_i(Y_i)}(\theta)\,\mathrm{d}\theta}{0.5\rho A V^2} \tag{4}$$

$$C_T = \frac{\frac{1}{2\pi}\int_{\theta}^{\theta+2\pi}\sum_{i=1}^{N} T_i(\theta)\,\mathrm{d}\theta}{0.5\rho A V^2 R} \tag{5}$$

Additionally, a torque amplitude coefficient is introduced here to quantify the magnitude of torque fluctuation over a revolution (Equation (6)).

$$C_{|T|} = \frac{T_{\max} - T_{\min}}{0.5\rho A V^2 R} \tag{6}$$

Finally, the turbine's overall performance is measured via the power coefficient, conventionally defined as in Equation (7).

$$C_{\mathrm{P}} = \frac{P}{0.5\rho A V^3} = \frac{\frac{1}{2\pi}\int_{\theta}^{\theta+2\pi}\left(\Omega\sum_{i=1}^{N} T_i(\theta)\,\mathrm{d}\theta\right)}{0.5\rho A V^3} \tag{7}$$

In the preceding equations, T_i is the instantaneous torque of a blade (N · m); $T_{\max(\min)}$ is the maximum (minimum) instantaneous torque (N·m); F_{Xi} and F_{Yi} are the thrust force and the lateral force acting on a blade (N); i is the blade index; θ is the azimuthal angle (rad); α is angle of attack (°); A is the projected turbine area (m^2) (A= H·2R), and Ω is the angular velocity (rad/s).

3 Numerical modeling

3.1 Computational domain and numerical approach

The computational domain and mesh were defined following previous studies carried out by the authors on several hydrokinetic water turbines (Nguyen et al., 2021; Balduzzi et al., 2016a; Balduzzi et al., 2016b; Nguyen et al., 2020). Therefore, only a brief description is presented here.

The numerical simulations were carried out using the Ansys Fluent commercial software by solving the unsteady Reynolds-averaged Navier-Stokes (U-RANS) equations with the k-ω SST turbulence model. The coupled method was adopted for pressure-velocity coupling.

Regarding the dimensions of the open-field domain, the external boundaries must be placed at a sufficient distance from the turbine to avoid blockage effects in the lateral direction and to ensure a fully developed wake. In this study, the computational domain extends 60 times the rotor radius upstream of the rotor center and 120 times the rotor radius downstream (as shown in Figure 2). The domain consists of two zones, an inner rotating zone and an outer stationary zone, connected by a sliding interface with a radius 1.5 times greater than the turbine radius.

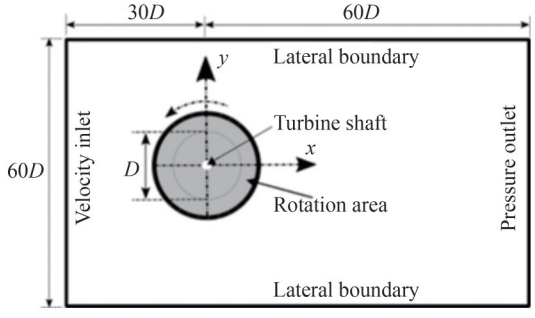

Figure 2 Schematic of the computational domain (figure not to scale)

The velocity of the incoming flow was obtained from the experimental measurements reported in Nguyen et al. (2021) and Lundin et al. (2013). A uniform velocity of 1.4 m/s (realistic for hydrokinetic turbines installed in rivers) was applied to the inlet boundary. Turbulent intensity was set to 5%, and the turbulent length scale was set to 1 m. Ambient pressure was imposed at the outlet boundary.

Figure 3 presents the unstructured mesh adopted for the entire domain, progressively refined toward the rotor region. To properly capture the development and mixing of the wake behind the rotor, a drop-shaped refinement region was defined, as shown in Figure 3(a). For each blade, an additional circular refinement enclosing the blade with a radius equal to the chord length was also implemented (Figure 3(b)). In compliance with the requirements of the k-ω SST turbulence model, the wall-adjacent cell size was dimensioned to guarantee a dimensionless wall distance (y^+) on the order of ~1. The boundary layer region was captured by introducing 32 layers with a growth rate of 1.1 (Figure 3(c)).

3.2 Verification and validation of the CFD model

In this section, the CFD model is first verified numerically (i.e., the suitability of the mesh, time step, and convergence criteria is assessed) and then validated using unique experimental data from a 5-blade turbine tested in a river by Uppsala University, which also served as the baseline geometry for the verification analyses. Unlike other studies in the literature, which lack experimental validation or rely on scale models in a laboratory environment, this approach affords a much higher degree of confidence in the suitability of the numerical approach. The geo-

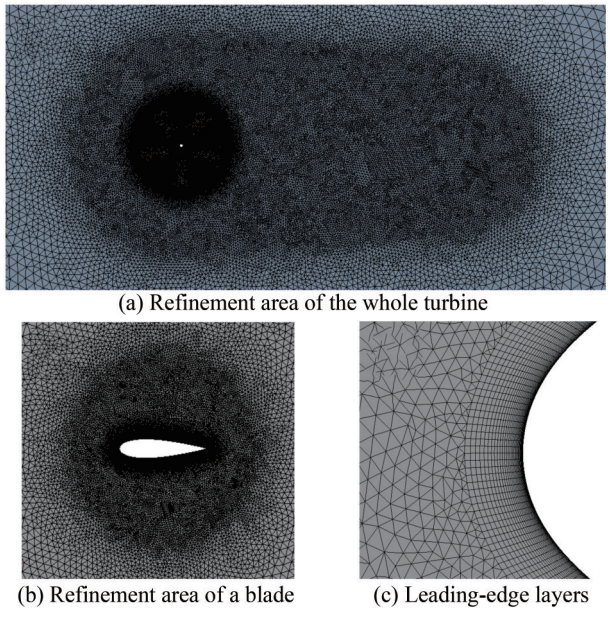

Figure 3 Computational meshes

metrical and operational parameters of the reference 5-blade turbine are presented in Table 3. Additionally, it is worth noting that for a similar 3-blade configuration, the verification and validation process has been extensively examined in a previous publication, as detailed in Nguyen et al. (2020).

Table 3 Reference turbine model parameters

N	R (m)	c (m)	Blade profile	σ	P (kW)	TSR	V (m/s)
5	2.94	0.18	NACA 0021	0.153	7.5	2.0 – 4.0	1.4

Based on previous experience, three different grids were considered: a coarse mesh (~3.0×10^5 elements), a medium mesh (~5.2×10^5 elements), and a fine mesh (~7.0×10^5 elements). Convergence was assessed by analyzing the torque profile over a revolution. As shown in Figure 4, no notable difference in torque results between the medium and fine meshes is observed, corresponding to a difference in the aggregate torque profile over a revolution of less than 0.08%. The medium mesh with 5.2×10^5 elements was therefore selected owing to its optimal compromise between prediction accuracy and computational cost.

It is also worth noting that the analysis presented in Figure 4 was based on fully converged torque profiles, as demonstrated by Figure 5, which shows the convergence history of the average power over 40 revolutions in terms of relative change against the value achieved at the last revolution. After reaching the 30th revolution, no considerable difference (below 0.3%) is observed between two subsequent revolutions. All simulations reported in the present study were run for 30 or more revolutions to achieve the same convergence threshold.

Another key parameter requiring verification is the time step selection. Figure 6 shows the instantaneous torque against the azimuthal angle for different values of the

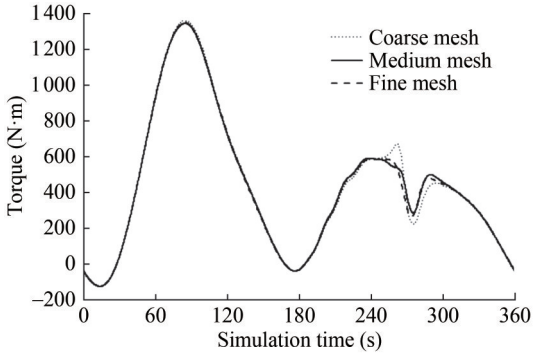

Figure 4 Mesh independence study

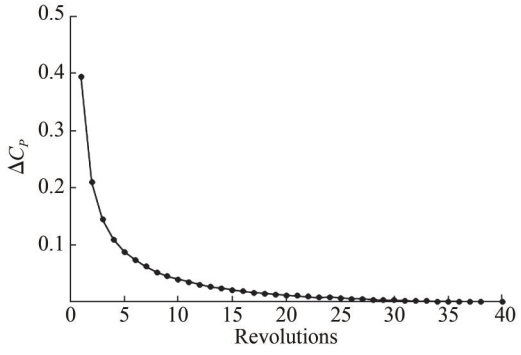

Figure 5 Convergence with respect to the number of simulated revolutions

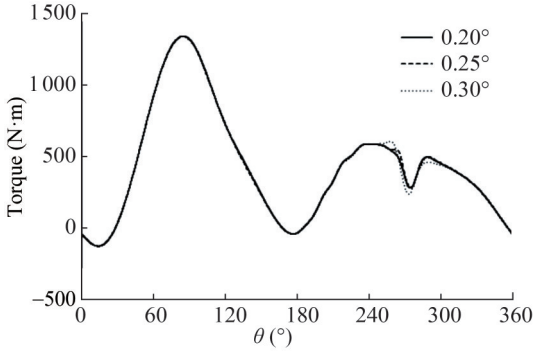

Figure 6 Time step independence study (reported as azimuthal angle variation)

angular step ($d\theta_1 = 0.2°$, $d\theta_2 = 0.25°$, $d\theta_3 = 0.3°$). The results indicate a slight difference in the azimuthal angular range $\theta = 240°–300°$, which can be attributed to the interaction between the blades and the wake of the central shaft occurring around $\theta = 270°$. Although the difference between $d\theta_1 = 0.2°$ and $d\theta_2 = 0.25°$ in terms of average torque is almost negligible (0.005 4%), to capture the aforementioned unsteady flow interaction (especially for configurations with a large number of blades) with high accuracy, the azimuthal step $d\theta = 0.2°$ was selected for all simulations in the present study.

As discussed, final validation of the CFD model was performed by comparing the power coefficient values between numerical predictions and experimental data. The

field-measurement campaign was conducted on the Dalälven River by the Marine Current Research Group at Uppsala University. A 5-blade turbine with a 5 m blade height and 2.94 m radius was tested in a 7 m deep river. Details of the experimental test and data collection can be found in Lundin et al. (2013) and Yuen et al. (2011). Here, only the final power output obtained from the test and the resistance torque caused by system losses are considered for comparison with the numerical results. The system power losses are accounted for during the post-processing of the 2D simulations by subtracting them from the numerical hydrodynamic power, thereby obtaining the power at the generator shaft. While it is undeniable that 2D simulations such as those presented here may fail to predict some three-dimensional effects present in the real turbine, the comparison presented in Figure 7 is consistent with the prescription in Bianchini et al. (2017) and is therefore considered a meaningful validation. It shows good agreement between the calculated and experimental power coefficients. The trend of C_P as a function of TSR is captured reasonably well, especially at moderate TSRs (TSR = 3.0–3.5), with small deviations compared to the measurements. To quantify the relative error between measurements and numerical results, the difference between the experimental torque and the 2D CFD simulation at TSR = 3.1 is 1.7%. The validated CFD model was therefore considered a reliable tool for the parametric numerical analyses of the present study.

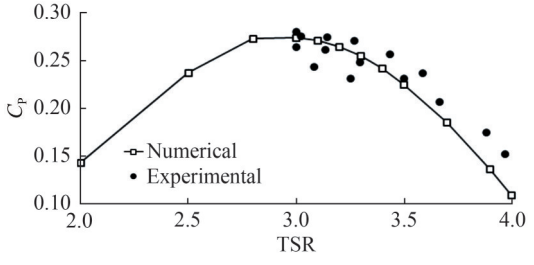

Figure 7 Model validation against measurements: power coefficient against TSR

4 Results and discussion

In this section, the main findings of the study are presented for the 16 turbine configurations. As discussed in the Introduction, two levels of analysis are proposed.

In the first, the impact of macro design parameters on turbine performance is examined. The focus is placed not only on power output and the influence of merit figures such as blade number, blade-chord length, Reynolds number, and optimal TSR but also on the overall torque fluctuation over a revolution. This figure is particularly relevant to hydrokinetic VATs; unlike their wind counterparts, the impact of centrifugal loads in VATs is much lower relative to hydrodynamic ones. These forces fluctuate considerably over a revolution, leading to strong pulsations in the thrust force acting on the supporting tower, which in turn cause fatigue loading and reliability issues.

In the second level of analysis, the aforementioned results are interpreted from a hydrodynamic standpoint, with the focus shifting to modifications in the single-blade torque profile and, primarily, to the unsteady fluid dynamics at the blade level, which are analyzed here using an innovative method of sampling the equivalent angle of attack and compensating for virtual cambering.

4.1 Effect of blade number

In this section, the influence of the number of blades is analyzed for different values of the turbine solidity while keeping the turbine radius constant at 2.94 m (see the resulting 12 configurations in Table 4). The rationale for this analysis is to investigate which turbine configuration yields the best performance for a given reference swept area and hence a target rated power. While the three-blade turbine is known to be the optimum in wind energy applications, studies on hydrokinetic rotors have reported different results, ranging from 2-blade rotors preferred for higher efficiency (Balduzzi et al., 2021) to higher blade numbers preferred for reduced torque fluctuations. Considering typical river flow conditions, the flow velocity is set to 1.4 m/s for all simulations, while the rotational speed is varied to correspond to TSR values ranging from 2.0 to 4.5. In the present study, the 2-blade configuration was not considered, as field experience demonstrated that mechanical stresses on blades of this size are excessive.

Table 4 Blade-chord values for the 12 geometric configurations tested (m)

N	Blade chord values		
	$\sigma = 0.102$	$\sigma = 0.153$	$\sigma = 0.204$
3-blade	0.20	0.300	0.40
4-blade	0.15	0.225	0.30
5-blade	0.12	0.180	0.24
6-blade	0.10	0.150	0.20

Figure 8(a) illustrates the trends in the power coefficient and torque amplitude coefficient as a function of TSR with an increasing number of blades at a fixed solidity of σ = 0.102. As a first outcome, the maximum power coefficient increases almost linearly as the number of blades is reduced, from 0.369 for the 6-blade case to 0.398 for the 3-blade case, representing a 7.9% increase in performance. In addition, the shift in the C_P value is nearly constant across the entire range of TSRs analyzed. As is also apparent from Figures 8(c) and 8(e), similar conclusions can be drawn at higher solidities (σ = 0.153, 0.204). In these configurations, the maximum C_P differs by up to 4.3% and 3.6% for σ = 0.153 and σ = 0.204, respectively, when

the blade number is reduced from 6 to 3. This aligns well with previous experience in wind energy applications, confirming that, notwithstanding fluid viscosity, the C_P is inversely proportional to the number of blades at a given solidity. In agreement with the literature, the optimal TSR also decreased with increasing solidity (at σ = 0.102, 0.153, and 0.204, the C_P reaches its maximum value at TSR = 4.0, 3.4, and 2.8, respectively).

Focusing now on the 3-blade rotor, which showed the best performance across all solidities, the maximum power coefficient also increased with solidity (from 0.400 to 0.420 to 0.426). While common design guidelines suggest the opposite (i. e., an increase in peak efficiency with lower solidities), this trend can be attributed to a combination of factors. On the one hand, increasing the chord at a constant radius means that the chord-based Reynolds number (Re_c) increases, and in turn, likely the efficiency of the airfoil. For reference, the Re_c at 0° azimuthal angle, no induction, and optimal TSR ranges from 1.5 M to 2 M to 2.5 M for the cases considered. The impact on aerodynamics in this range is expected to be present but moderate, as will be shown in the next section. More importantly, what is often overlooked in this type of analysis is the impact of flow curvature effects, and primarily virtual camber (Rainbird et al., 2015). When increasing the chord at a constant radius, the chord-to-radius ratio (c/R) also increases; this ratio is the controlling parameter for this effect, as it determines how much the local relative velocity varies along the airfoil. The higher the c/R, the more curved is the outward camber of the virtual airfoil. For the cases analyzed here, the c/R varies from 0.068 to 0.102 to 0.136. Previous studies (Rainbird et al., 2015) showed that for values exceeding 0.1, this effect becomes predominant in airfoil performance. While it cannot be stated a priori whether the change in aerodynamic characteristics of the airfoil will lead to an increase or decrease in overall efficiency, it is certainly responsible for higher blade loading at low TSRs (the virtual airfoil has higher camber and higher glide at higher angles of attack, which are reached earlier by the turbine), which in turn shifts the optimal TSR to lower values. Figure 9 compares the lift coefficient and glide coefficient for the virtual airfoils at the corresponding reference Reynolds number; static polars are obtained with XFoil (XFOIL, 2026) with N_{crit} = 9. While Section 4.3 will provide an overview of the actual dynamic polars in motion onboard the VAT, the static data presented here are nonetheless useful for illustrating the impact of such changes on the airfoil aerodynamics.

Shifting attention from the global power coefficient to the torque fluctuations over a single revolution, a major difference between wind and hydrokinetic turbines must be noted. The rotational energy stored in a hydrokinetic turbine is, on a relative basis, much lower than that of a wind turbine. This can be understood from the fact that the

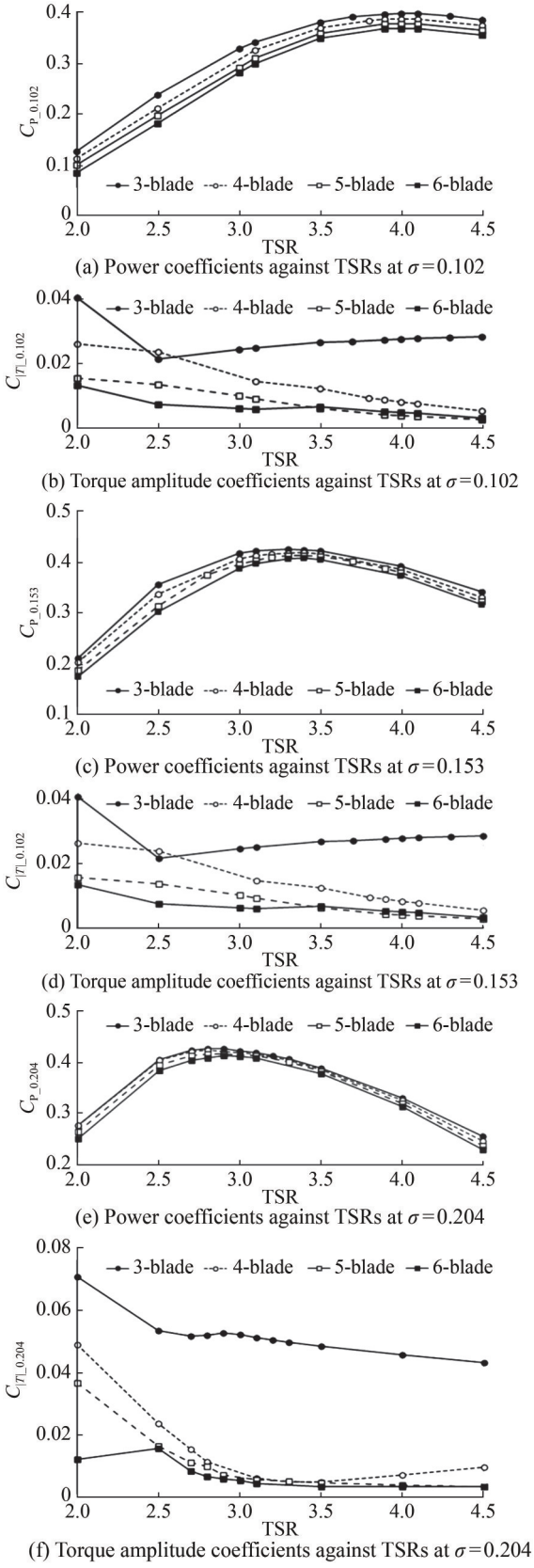

(a) Power coefficients against TSRs at σ=0.102

(b) Torque amplitude coefficients against TSRs at σ=0.102

(c) Power coefficients against TSRs at σ=0.153

(d) Torque amplitude coefficients against TSRs at σ=0.153

(e) Power coefficients against TSRs at σ=0.204

(f) Torque amplitude coefficients against TSRs at σ=0.204

Figure 8 Power coefficients and torque amplitude coefficients against TSRs at solidity values of σ = 0.102, σ = 0.153, and σ = 0.204; solidity is varied by modifying the chord

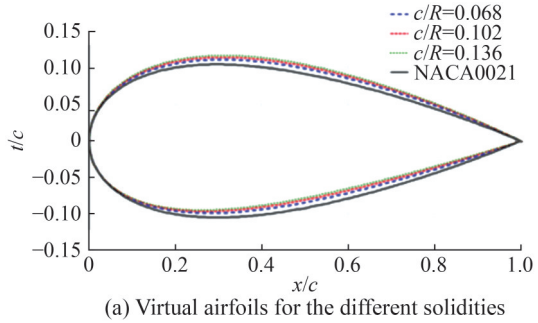

(a) Virtual airfoils for the different solidities

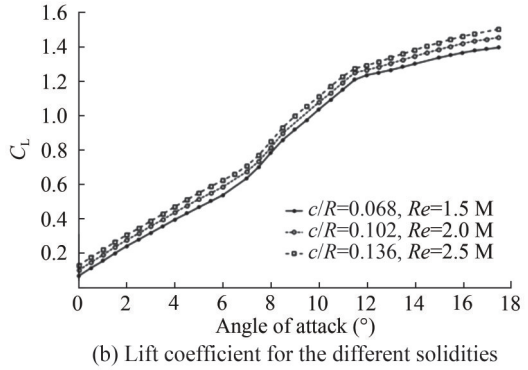

(b) Lift coefficient for the different solidities

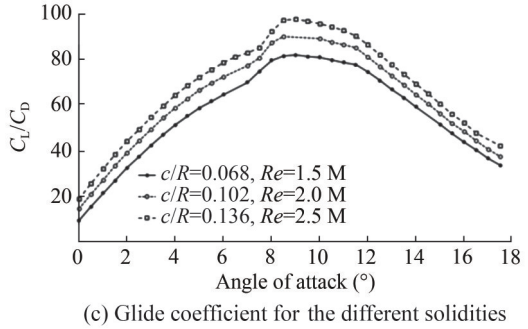

(c) Glide coefficient for the different solidities

Figure 9 Virtual airfoils for the different solidities and corresponding lift and glide coefficients for the configurations analyzed in the study

density of the blades is of a similar order as the fluid density in water, whereas the blades of a wind turbine are considerably heavier than air. As an example, the experimental turbine operated by Uppsala University in Söderfors is rated at 7.5 kW at approximately 15 r/min and has an estimated moment of inertia of 3 000 kg·m^2 (Yuen et al., 2011). This means that the stored rotational energy of the turbine corresponds to only 0.5 s of operation at full power, or 1/8 of a revolution. Consequently, the turbine changes its rotational velocity very easily, and it cannot be expected to act as a buffer for torque variations, as is traditionally the case for a wind turbine. This makes it important to maintain low torque variations for smooth turbine operation without excessively large fluctuations in power output and rotational speed. From this perspective, a smooth torque profile is also pivotal for containing fatigue loading on the shaft. To this end, the coefficient of torque amplitude ($C_{|T|}$) has been compared across different cases with varying numbers of blades (Figures 8(b), 8(d), and 8(f)). The figures confirm the general trend that low TSRs produce larger torque variations; when moving from 3 to 4 blades, the fluctuations decrease drastically, while beyond this value, the reduction is modest. The torque fluctuations also become smaller at high TSRs owing to a narrower range of angle of attack experienced over the revolution. However, it should be noted that turbines with high solidity are designed to operate at lower TSRs, so there are still improvements in torque smoothing when increasing the number of blades in these cases. The general recommendation is that if reducing the torque amplitude is necessary, using 4 blades instead of 3 is beneficial.

4.2 Effect of the reynolds number

As shown by the previous analyses, the variation in turbine efficiency was always associated with a simultaneous increase in both Re_c and the c/R ratio (at least within the ranges investigated here). To isolate and better understand the effects of the Reynolds number alone, this section presents the results of upscaled turbines and their comparison with the original-scale turbines. Starting from the configurations with solidity $\sigma = 0.204$, which showed superior performance, the values of chord length, turbine radius, and shaft radius are scaled by a factor of 2. As a result, the Re_c values at a given TSR are doubled, since the parameters c and R are twice the original ones while the rotational speed is halved. The parameters for each case are listed in Table 5.

Table 5 Study cases for analyzing the reynolds number effect

N	σ	R (m)	c (m)	Re_c (×10^5)	TSR
3-blade	0.204	2.94	0.40	11.1–25.0	2.0–4.5
		5.88	0.80	22.2–50.0	
4-blade		2.94	0.30	8.4–18.8	
		5.88	0.60	16.8–37.6	
5-blade		2.94	0.24	6.7–15.0	
		5.88	0.48	13.4–30.0	
6-blade		2.94	0.20	5.6–12.5	
		5.88	0.40	11.2–25.0	

Figure 10 shows the trends in C_P as a function of TSR for all configurations with 3 to 6 blades at higher Re_c. In addition, to better highlight the effect of Re_c alone, the curves for the original 3-blade and 6-blade configurations are also shown. For the newly tested cases, the maximum C_P at the optimal TSR is 1.6% higher for the 3-blade case compared with the 6-blade case. This difference increases to roughly 5% under off-design conditions, both at high and low TSRs. It is worth noting that at high Re_c values, the 3-blade and 4-blade rotors exhibit nearly equivalent performance, and the results are generally less sensitive to the number of blades.

When comparing the upscaled turbine with the original-

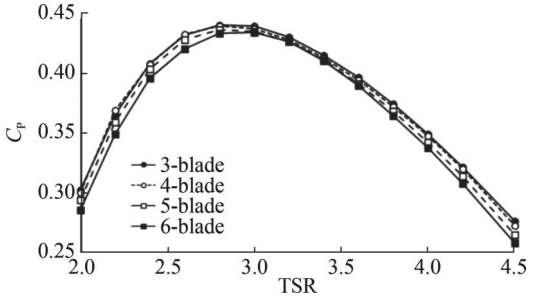

Figure 10 Power coefficient against TSR at σ = 0.204 for the upscaled turbines. Results can be compared with Figure 8(e)

size turbine, the efficiency benefits arising from the increase in Reynolds number are apparent. The increase in C_P for the upscaled turbine relative to the original is roughly 4.3% at the optimal TSR and up to 10% under off-design conditions. As an additional consideration, the 6-blade upscaled turbine and the 3-blade original-size turbine are characterized by the same Reynolds number conditions and solidity, and they provide very similar performance. More precisely, the 6-blade upscaled turbine has a slightly higher efficiency (+1.4%). The impact of the Reynolds number at the airfoil level will become clearer in Section 4.3 through the study of local unsteady aerodynamics.

Figure 11 shows the instantaneous torque coefficient at the optimal TSR of each turbine over a revolution. With the increase in the number of blades from 3 to 6, the torque amplitude variation decreases from 18.5% to 1.5%, respectively.

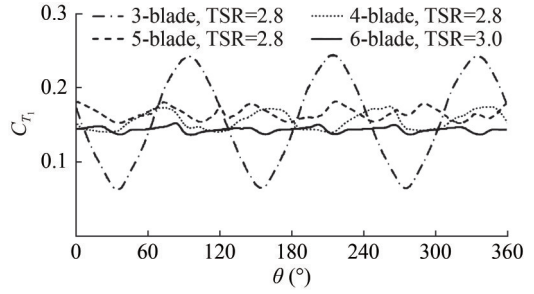

Figure 11 Instantaneous torque coefficient of the upscaled turbines at their respective optimal TSRs vs. azimuth at σ = 0.204

Figure 12 presents the coefficient of torque amplitude for the upscaled turbine against TSR. The torque at high TSRs varies less than at low TSRs, indicating that operation at higher rotational speeds is more stable. The same behavior holds for the smaller turbine across different numbers of blades. However, the 3-blade turbine exhibits considerably higher torque variation than the 4-, 5-, and 6-blade configurations. This observation underscores the importance of selecting the optimal number of blades in the turbine design process for marine current applications, as reducing torque fluctuations could enhance turbine longevity.

As a final analysis, the maximum C_P for each tested geometrical configuration is plotted in Figure 13 to summarize and visualize the global effect of solidity and Reynolds number on the turbine's hydrodynamic performance. From the figure, it is apparent that the reduction of C_P with increasing number of blades is less pronounced for cases at higher solidity or higher Re_c.

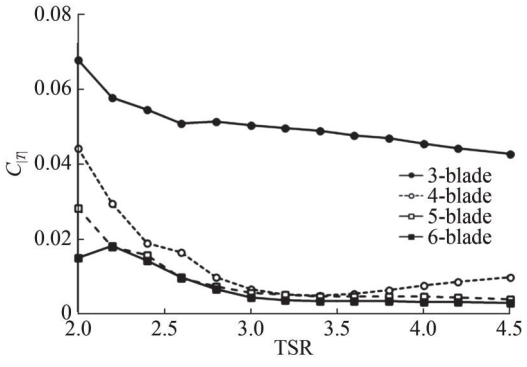

Figure 12 Torque amplitude coefficients of the upscaled turbines against TSR at σ = 0.204

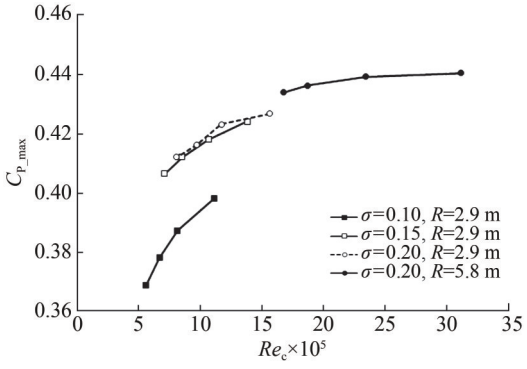

Figure 13 Global effect of solidity and Reynolds number on the turbine's hydrodynamic performance

By reporting the same C_P results as a function of the revolution-averaged Re_c, additional considerations can be made. The low-solidity case is more sensitive to the number of blades since the turbine operates in a range of Re_c close to the laminar threshold, whereas the σ = 0.20, R = 5.88 m case starts to exhibit Reynolds-independent behavior. For the same reason, increasing the solidity from 0.10 to 0.15 provides substantial benefits, while the further gain from an increase to σ = 0.20 is less marked. To gain a comprehensive understanding of these aspects, a thorough analysis was conducted to examine the local dynamic phenomena occurring on the hydrofoils.

At the end of this section, however, it is important to place the results in the proper critical context. As will be shown in the following section, the discussed results at the turbine level stem from improved aerodynamic performance of the airfoils with increasing Re_c, which enables them not only to reach a higher maximum glide ratio but also greater resistance to stall, which underlies the flatter torque profiles shown in Figure 11. These effects are known from past experience with wind-driven VATs and will

asymptotically diminish at even higher Reynolds numbers, where the airfoil performance becomes nearly Reynolds-independent. However, the present results are considered of interest to the scientific community working on hydrokinetic VATs, since the ranges investigated in this study are typical of the designs under study for rivers and thus highlight how even small changes in Re_c can be consequential within these ranges.

4.3 Unsteady aerodynamics

The analysis of the results presented so far has described the behavior of the different geometrical configurations and attempted to relate variations in efficiency to the main parameters considered in the study. The present section instead aims to provide deeper insight into the hydrodynamics of the hydrofoils to aid the interpretation of these results. All curves shown in the following figures correspond to the condition of maximum C_P, i. e., the optimal TSR.

Starting with the instantaneous torque produced by a single blade, Figure 14 shows the trend of the tangential force coefficient (C_{TANG}) over one revolution for the σ = 0.10 case, which was found to be the most sensitive to variations in blade number. In this context, the tangential force coefficient is preferred over the torque coefficient because it is normalized by the blade chord, enabling a more effective comparison of torque-extraction efficiency among blades with different chord lengths. The results show that when the number of blades is reduced, and the chord length is consequently increased, torque production over the entire upwind portion of the rotation is enhanced, leading to an increase in the torque peak of up to 16%, along with a forward shift of approximately 4°. This outcome results from the combined increase in both the Reynolds number and the c/R ratio, which explains the higher C_P values obtained.

This behavior is first qualitatively analyzed by comparing the relative velocity flow fields around the blade at an azimuthal position of 90° for the two extreme cases, namely the 3-blade and 6-blade configurations, as shown in Figure 15. The relative velocity is shown in terms of velocity deficit normalized by the inlet velocity. The effect of the increased Reynolds number is particularly evident on the suction side near the trailing edge, where the thickness of the separated region is more pronounced for the 6-blade case. Conversely, the effect of the increased virtual camber in the 3-blade configuration can be observed in the higher flow acceleration on the suction side near the leading edge, as well as in the greater deflection of the wake.

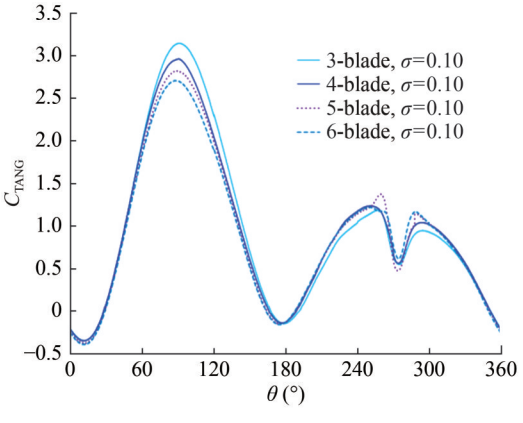

Figure 14 Instantaneous tangential force coefficient against azimuth at TSR_{opt} for $\sigma = 0.10$

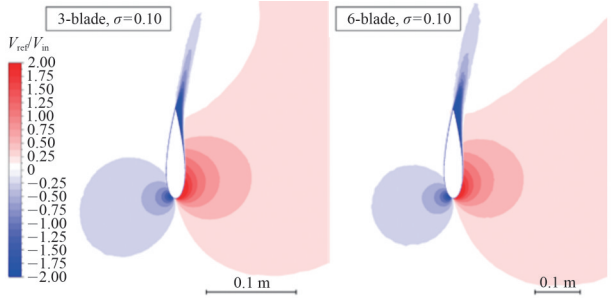

Figure 15 Normalized relative velocity deficit contours at TSR_{opt} for $\sigma = 0.10$, azimuthal position $\theta = 90°$

To better elucidate the physics underlying the analyzed trends, dynamic lift and drag polars were reconstructed for a more comprehensive understanding of the hydrodynamic force output. To this end, the solved flow-field data were post-processed to extract the actual flow incidence experienced by the blade and to sample the local relative velocities. The procedure for computing the instantaneous local incidence, presented and adopted by Melani et al. (2020), enabled the computation of the dynamic lift and drag polars.

The resulting lift polars for the σ = 0.10, σ = 0.15, and σ = 0.20 cases are reported in Figures 16–18, respectively. Overall, the three figures exhibit similar behavior in terms of both the dynamic trend of the polars and the variation of the curves with the number of blades. The main dynamic features are highlighted in Figure 16. In the windward portion of the rotation, the angle of attack (AoA) increases (pitch-up phase), and the lift coefficient follows a curve

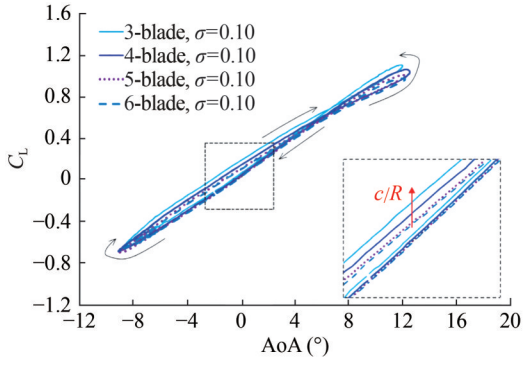

Figure 16 Dynamic lift coefficient against AoA at TSR_{opt} for $\sigma = 0.10$

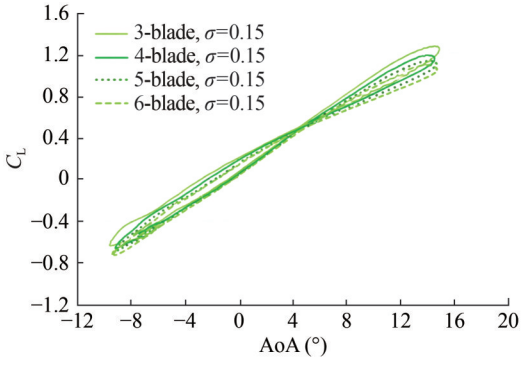

Figure 17 Dynamic lift coefficient against AoA at TSR_{opt} for $\sigma = 0.15$

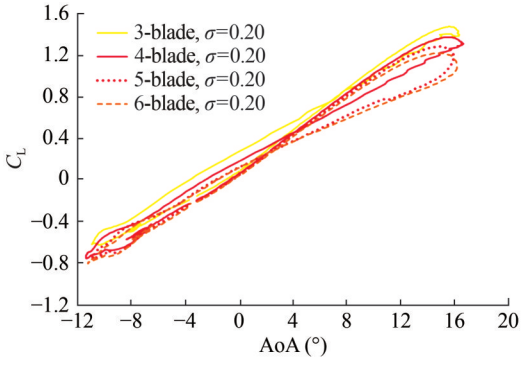

Figure 18 Dynamic lift coefficient against AoA at TSR_{opt} for σ =0.20

that depends on the virtual camber effect (Rainbird et al., 2015). Despite the hydrofoil being symmetrical, the C_L value at AoA = 0° exceeds zero for all configurations owing to this virtual camber effect, which becomes more pronounced as the number of blades decreases, attributed to the higher c/R ratio. This behavior is emphasized in the zoomed-in section: the higher the chord, the greater the lift value at AoA = 0°. Subsequently, after reaching the maximum AoA, a dynamic effect becomes visible: when the pitch-down phase begins, the lift does not instantaneously decrease as the AoA decreases. This hysteresis effect results in a peak C_L that is higher for the 3-blade case owing to the higher Reynolds number. In summary, the combination of the virtual camber effect and the higher Reynolds number causes the dynamic lift polar to shift globally toward higher values when the number of blades is reduced, and the chord is increased at a given solidity. This observation justifies the trends in C_{TANG} shown in Figure 14 and, therefore, the enhanced power production reported in the previous section.

Finally, Figures 19 and 20 show a comparison of dynamic lift and drag polars for the 4-blade configurations to better highlight the effect of solidity. It is first worth noting that the range of AoAs is not the same for these curves, since they do not correspond to the same optimal TSR. The σ = 0.20 geometry allows higher AoA values without incurring stall effects, resulting in a maximum C_L of approximately 1.37. This superior performance compared with the lower-

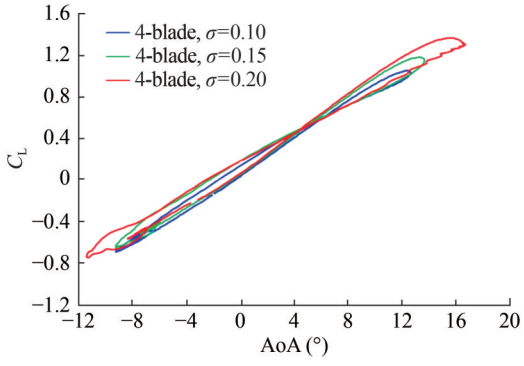

Figure 19 Dynamic lift coefficient against AoA at TSR_{opt} for the 4-blade cases

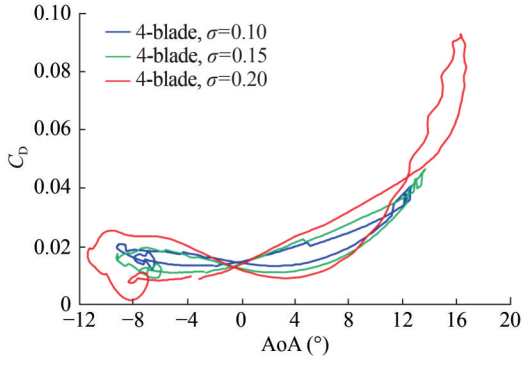

Figure 20 Dynamic drag coefficient against AoA at TSR_{opt} for the 4-blade cases

solidity cases is attributed to the stall delay phenomenon. On the other hand, the dynamic drag polars indicate that the $\sigma = 0.20$ case begins to suffer from non-negligible separation, as the maximum C_D is more than doubled. This behavior partly offsets the benefits achieved in terms of lift, justifying the small performance gap relative to the $\sigma = 0.15$ case. A further increase in solidity would shift the C_P peak toward an even lower optimal TSR, leading to a deterioration in performance as the separation effect becomes dominant.

4.4 Definition of best design compromises

In the previous sections, the 3-blade turbine configurations exhibited the highest power extraction across all solidity values, whereas the 6-blade turbine configurations provided the best performance in minimizing torque fluctuations. This section focuses on analyzing the results under optimal conditions

Figure 21 summarizes the configurations of blade number, blade-chord length, turbine radius, and local Reynolds number that optimize turbine performance, along with their optimal TSRs, at three constant solidity values. The power coefficient was taken from the maximum value observed in each case study, while the corresponding optimal TSR and the coefficient of torque amplitude ($C_{|T|}$) were extracted and

plotted as functions of blade number. It is apparent that the optimal TSR remains nearly constant regardless of the blade number at a given solidity (Figure 21(a)). In other words, the optimal TSR is primarily governed by rotor solidity and is independent of blade number, with the effect of Re_c being almost negligible. Conversely, the blade number has an almost linear effect on the optimal power coefficient (Figure 21(b)). The variation in optimal C_P from a high (6) to a low (3) blade number shows a relative increase of 7.9%, 4.3%, 3.6%, and 1.5% for solidity values of σ = 0.10, 0.15, 0.20, and σ = 0.20 for the scaled-up turbine, respectively. At higher solidity values, the impact of blade number on performance diminishes as the turbine approaches Reynolds-number-independent behavior. When the blade number is increased at constant solidity, the TSR_{opt} remains constant, and the C_P slightly decreases, but the $C_{|T|}$ is strongly reduced (Figure 21(c)).

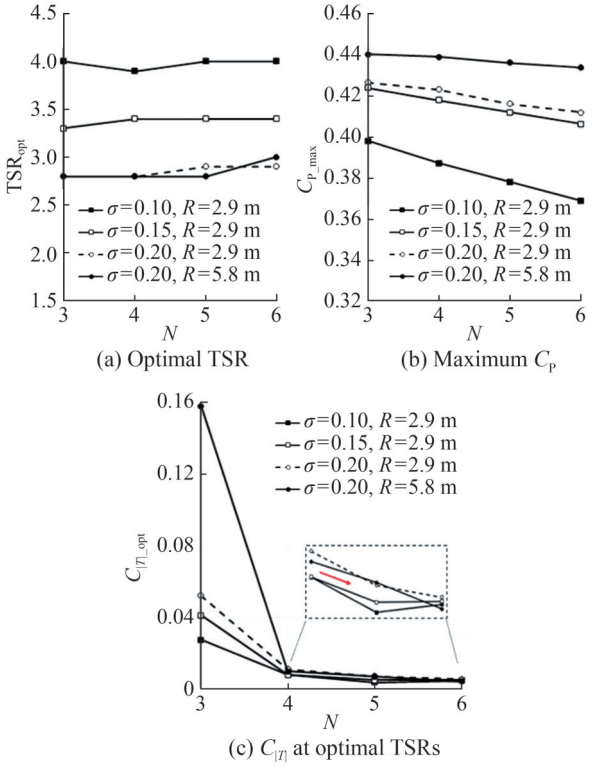

Figure 21 Influence of blade number on the optimal TSR, maximum C_P, and $C_{|T|}$ at optimal TSRs

5 Conclusions

This paper presents a numerical analysis of the effects of operational and geometric characteristics on energy performance and hydrodynamic forces across 16 vertical-axis turbine configurations with three fixed solidities in both original and upscaled turbine sizes for marine current applications. These configurations vary in the number of blades, chord length, turbine solidity, diameter, TSRs, and Reynolds number. At a given solidity, the effect of changing the number of blades, and hence the blade chord, on performance was assessed for each configuration. The selected configurations are relevant to the sizes of utility-scale hydrokinetic turbines for rivers or channels currently under study by the emerging industry in this sector.

In terms of power performance, the results consistently indicate that, as known from wind energy applications of VATs, the 3-blade turbine design outperforms configurations with 4, 5, or 6 blades, achieving the highest power coefficient. Additionally, the results showed that the maximum efficiency (roughly 43%) was achieved with the 3-blade configuration at the highest solidity tested (σ = 0.20). By analyzing the C_P trends against TSR as a function of the Reynolds number, along with dynamic lift and drag polars, the physical mechanisms driving this outcome were identified. At a given solidity, the increase in chord length when reducing the number of blades leads to

- A negligible effect on the optimal TSR; therefore, the peripheral speed at maximum C_P remains constant;
- A higher Reynolds number, with the benefit of greater resistance to separation when the AoA exceeds 10°;
- A higher c/R ratio, i.e., an increase in the virtual curvature effect, with the benefit of shifting the overall dynamic lift polar toward higher values (at least within the ranges of c/R investigated herein).

Similar considerations apply when analyzing the results for a given number of blades. An increase in chord length to raise the solidity produces the same effects as operating at higher values of both the Reynolds number and c/R. However, in this case, the optimal TSR is progressively shifted toward lower values. As a result, the increase in the Reynolds number is partially mitigated and, moreover, the range of AoAs experienced by the blade profile becomes wider, approaching stall conditions. It was found that the σ = 0.20 geometry allows higher AoA values without incurring stall effects, resulting in a maximum lift coefficient of 1.37 under dynamic conditions.

Regarding torque fluctuation, the high-blade-number turbine configuration emerges as the optimal design, especially the 6-blade turbine of medium or commercial size, which exhibits the lowest torque variation among all cases. This is particularly relevant for turbines operating at high TSRs (above 3.0), where torque fluctuation in high-blade-number turbines (4, 5, or 6 blades) becomes largely independent of structural parameters such as blade number, chord length, and turbine radius. Consequently, turbines with a high number of blades can reduce the number of optimal design constraints during the engineering process. These findings provide new insights into turbine scale-up factors for medium- and commercial-sized turbines, aiding researchers and designers in optimizing marine current power extraction.

Nomenclature

Acronyms	
CFD	Computational fluid dynamics
HATs	Horizontal-axis turbines
NACA	National advisory committee for aeronautics
TSR	Tip speed ratio
TSR_{opt}	Optimal tip speed ratio
SST	Shear stress transport
URANS	Unsteady Reynolds-averaged Navier-Stokes
VATs	Vertical-axis turbines
Greek symbols	
Ω (rad/s)	Angular velocity
α (°)	Angle of attack
θ (°)	Azimuthal angle
β (°)	Pitch angle
Latin symbols	
F_{xi}, F_{yi} (N)	Vertical and horizontal forces of the blade
F_n, F_t (N)	Normal and Tangential forces of the blade
T (N·m)	Average torque acting on the turbine
C_P	Turbine power coefficient
C_T	Torque coefficient
$C_{\|T\|}$	Coefficient of torque amplitude
C_{Ti}	Coefficient of instantaneous torque
C_L	Lift coefficient
C_D	Drag coefficient
C_{TANG}	Tangential force coefficient
N	Number of blades
D (m)	Rotor diameter
H (m)	Turbine height
R (m)	Rotor radius
c (m)	Blade chord
Re_c	Chord-based Reynolds number
y^+	Dimensionless wall distance
P (kW)	Rated power
V (m/s)	Water speed

Funding Open access funding provided by Uppsala University.

Acknowledgments The project was conducted with the support of STandUP for Energy. The computations were enabled by resources provided by the National Academic Infrastructure for Computing in Sweden (NAISS), partially funded by the Swedish Research Council through user agreement no. LiU-2022-05165.

Competing interests The authors have no competing interests to declare that are relevant to the content of this article.

References

Allan J, Bansard J, Jones N, Luomi M, Tan JM, Sun Y(2021) Glasgow Climate Change Conference: 31 October-13 November 2021. New York: IISD Earth Negotiations Bulletin 12: 1-40

Allen M, Antwi-Agyei P, Aragon-Durand F, Babiker M, Bertoldi P, Bind M, Brown S, Buckeridge M, Camilloni I, Cartwright A, Cramer W, Dasgupta P, Diedhiou A, Djalante R, Dong W, Ebi KL, Engelbrecht F, Fifita S, Ford J, Fuß S, et al. (2019) Global warming of 1.5 ℃: An IPCC special report on the impacts of global warming of 1.5 ℃ above pre-industrial levels and related global greenhouse gas emission pathways, in the context of strengthening the global response to the threat of climate change, sustainable development, and efforts to eradicate poverty. Laxenburg: International Institute for Applied Systems Analysis. https://pure.iiasa.ac.at/15716

Bachant P, Wosnik M (2016) Effects of reynolds number on the energy conversion and near-wake dynamics of a high solidity vertical-axis cross-flow turbine. Energies 9(2):73. https://doi.org/10.3390/en9020073

Balduzzi F, Melani PF, Soraperra G, Brighenti A, Battisti L, Bianchini A (2021) Some design guidelines to adapt a Darrieus vertical axis turbine for use in hydrokinetic applications. E3S Web of Conferences 312. Paris:EDP Sciences 08017. https://doi.org/10.1051/e3sconf/202131208017

Balduzzi F, Bianchini A, Ferrara G, Ferrari L (2016a) Dimensionless numbers for the assessment of mesh and timestep requirements in CFD simulations of Darrieus wind turbines. Energy 97: 246-261. https://doi.org/10.1016/J.ENERGY.2015.12.111

Balduzzi F, Bianchini A, Maleci R, Ferrara G, Ferrari L (2016b) Critical issues in the CFD simulation of Darrieus wind turbines. Renew Energy 85: 419-435. https://doi.org/10.1016/J.RENENE.2015.06.048

Bianchini A, Balduzzi F, Bachant P, Ferrara G, Ferrari L (2017) Effectiveness of two-dimensional CFD simulations for Darrieus VAWTs: a combined numerical and experimental assessment. Energy Conversion and Management 136. https://doi.org/10.1016/j.enconman.2017.01.026

Divakaran U, Ajith Ramesh A, Mohammad A, Velamati RK (2021) Effect of helix angle on the performance of helical vertical axis wind turbine. Energies 14(2): 3931-24. https://doi.org/10.3390/en14020393

DNV (2021) Energy Transition Outlook 2022: A Global and Regional Forecast to 2050. Norway: DNV 1-39. https://energytransition.techint.com/media/1fmjo10p/dnv_energy_transition_outlook_2022_main_report.pdf

Gielen D, Boshell F, Saygin D, Bazilian MD, Wagner N, Gorini R (2019) The role of renewable energy in the global energy transformation. Energy Strategy Reviews 24: 38-50. https://doi.org/10.1016/J.ESR.2019.01.006.

Hand B, Kelly G, Cashman A (2017) Numerical simulation of a vertical axis wind turbine airfoil experiencing dynamic stall at high Reynolds numbers. Computers & Fluids 149: 12-30. https://doi.org/10.1016/J.COMPFLUID.2017.02.021

International Energy Agency (IEA) (2022) World Energy Outlook

2022. Paris: IEA. Https://Www.IeaOrg/Reports/World-Energy-Outlook-2022/Executive-Summary 2022: 524

Ismail MF, Vijayaraghavan K (2015) The effects of aerofoil profile modification on a vertical axis wind turbine performance. Energy 80: 20-31. https://doi.org/10.1016/J.ENERGY.2014.11.034

Jafari M, Razavi A, Mirhosseini M (2018) Effect of airfoil profile on aerodynamic performance and economic assessment of H-rotor vertical axis wind turbines. Energy 165(Part A): 792-810. https://doi.org/10.1016/j.energy.2018.09.124

Kamani D, Ardehali MM (2023) Long-term forecast of electrical energy consumption with considerations for solar and wind energy sources. Energy 268: 126617. https://doi.org/10.1016/j.energy.2023.126617

Leonardo P. Chamorro REAA, Sotriopulos F (2012) Reynolds number dependence of turbulence statistics in the wake of wind turbines. Wind Energy 15: 733-742. https://doi.org/10.1002/we.501

Li Y, Yang S, Feng F, Tagawa K (2023) A review on numerical simulation based on CFD technology of aerodynamic characteristics of straight-bladed vertical axis wind turbines. Energy Reports 9: 4360-4379. https://doi.org/10.1016/J.EGYR.2023.03.082

Li Q, Maeda T, Kamada Y, Murata J, Shimizu K, Ogasawara T, Nakai A, Kasuya T (2016) Effect of solidity on aerodynamic forces around straight-bladed vertical axis wind turbine by wind tunnel experiments (depending on number of blades). Renew Energy 96: 928-939. https://doi.org/10.1016/j.renene.2016.05.054

Lundin S, Forslund J, Carpman N, Grabbe M, Yuen K, Apelfröjd S, Goude A, Leijon M (2013) The Söderfors Project: Experimental Hydrokinetic Power Station Deployment and First Results. 10th European Wave and Tidal Energy Conference (EWTEC 2013). Aalborg: DiVA

Ma N, Lei H, Han Z, Zhou D, Bao Y, Zhang K, Zhou L, Chen C (2018) Airfoil optimization to improve power performance of a high-solidity vertical axis wind turbine at a moderate tip speed ratio. Energy 150: 236-252. https://doi.org/10.1016/j.energy.2018.02.115

McTavish S, Feszty D, Nitzsche F (2013) Evaluating Reynolds number effects in small-scale wind turbine experiments. Journal of Wind Engineering and Industrial Aerodynamics 120: 81-90. https://doi.org/10.1016/j.jweia.2013.07.006

Melani PF, Balduzzi F, Ferrara G, Bianchini A (2020) How to extract the angle attack on airfoils in cycloidal motion from a flow field solved with computational fluid dynamics? Development and verification of a robust computational procedure. Energy Conversion and Management 223:113284. https://doi.org/10.1016/j.enconman.2020.113284

Melikoglu M (2018) Current status and future of ocean energy sources: A global review. Ocean Engineering 148: 563-573. https://doi.org/10.1016/J.OCEANENG.2017.11.045

Miller MA, Duvvuri S, Hultmark M (2021) Solidity effects on the performance of vertical-axis wind turbines 1: E9. https://doi.org/10.1017/flo.2021.9

Newell RG, Raimi D, Aldana G (2019) Global Energy Outlook 2019: The Next Generation of Energy. https://www.rff.org/publications/reports/global-energy-outlook-2019/

Nguyen MT, Balduzzi F, Goude A (2021) Effect of pitch angle on power and hydrodynamics of a vertical axis turbine. Ocean Engineering 238:109335. https://doi.org/10.1016/J.OCEANENG.2021.109335

Nguyen MT, Balduzzi F, Bianchini A, Ferrara G, Goude A (2020) Evaluation of the unsteady aerodynamic forces acting on a vertical-axis turbine by means of numerical simulations and open site experiments. Journal of Wind Engineering and Industrial Aerodynamics 198:104093. https://doi.org/10.1016/J.JWEIA.2020.104093

OECD (2012) OECD environmental outlook to 2050. (2012-3-15) [2026-3-13] https://www.oecd.org/en/publications/oecd-environmental-outlook-to-2050_9789264122246-en.html

Rainbird JM, Bianchini A, Balduzzi F, Peiró J, Graham JMR, Ferrara G, Ferrari L (2015) On the influence of virtual camber effect on airfoil polars for use in simulations of Darrieus wind turbines. Energy Conversion and Management 106: 373-384. https://doi.org/10.1016/j.enconman.2015.09.053

Rezaeiha A, Montazeri H, Blocken B (2018) Towards optimal aerodynamic design of vertical axis wind turbines: Impact of solidity and number of blades. Energy 165(Part B): 1129-1148. https://doi.org/10.1016/j.energy.2018.09.192

Sagharichi A, Zamani M, Ghasemi A (2018) Effect of solidity on the performance of variable-pitch vertical axis wind turbine. Energy 161: 753-775. https://doi.org/10.1016/j.energy.2018.07.160

Subramanian A, Yogesh SA, Sivanandan H, Giri A, Vasudevan M, Mugundhan V, Velamati RK (2017) Effect of airfoil and solidity on performance of small scale vertical axis wind turbine using three dimensional CFD model. Energy 133: 179-190. https://doi.org/10.1016/j.energy.2017.05.118

Shukla V, Kaviti AK (2017) Performance evaluation of profile modifications on straight-bladed vertical axis wind turbine by energy and Spalart Allmaras models. Energy 126: 766-795. https://doi.org/10.1016/J.ENERGY.2017.03.071

Tong G, Li Y, Tagawa K, Feng F (2023) Effects of blade airfoil chord length and rotor diameter on aerodynamic performance of straight-bladed vertical axis wind turbines by numerical simulation. Energy 265:126325. https://doi.org/10.1016/j.energy.2022.126325

Walker JM, Flack KA, Lust EE, Schultz MP, Luznik L (2014) Experimental and numerical studies of blade roughness and fouling on marine current turbine performance. Renew Energy 66: 257-267. https://doi.org/10.1016/j.renene.2013.12.012

XFOIL (2026) XFOIL subsonic airfoil development system. [2025-12-23] https://web.mit.edu/drela/Public/web/xfoil/

Yuen K, Lundin S, Grabbe M, Lalander E, Goude A, Leijon M (2011) The Söderfors Project : Construction of an Experimental Hydrokinetic Power Station. The 9th European Wave and Tidal Energy Conference, Southampton. Southampton 5-9

Zamani M, Nazari S, Moshizi SA, Maghrebi MJ (2016a) Three dimensional simulation of J-shaped Darrieus vertical axis wind turbine. Energy 116(Part 1): 1243-1255. https://doi.org/10.1016/J.ENERGY.2016.10.031

Zamani M, Maghrebi MJ, Varedi SR (2016b) Starting torque improvement using J-shaped straight-bladed Darrieus vertical axis wind turbine by means of numerical simulation. Renewable Energy 95:109-126. https://doi.org/10.1016/J.RENENE.2016.03.069

Zanforlin S, Deluca S (2018) Effects of the Reynolds number and the tip losses on the optimal aspect ratio of straight-bladed Vertical Axis Wind Turbines. Energy 148:179-195. https://doi.org/10.1016/J.ENERGY.2018.01.132

Zhou Z, Benbouzid M, Charpentier JF, Scuiller F, Tang T (2017) Developments in large marine current turbine technologies – A review. Renewable and Sustainable Energy Reviews 71:852-858. https://doi.org/10.1016/J.RSER.2016.12.113

Zhu H, Hao W, Li C, Ding Q (2019) Numerical study of effect of solidity on vertical axis wind turbine with Gurney flap. Journal of Wind Engineering and Industrial Aerodynamics 186: 17-31. https://doi.org/10.1016/J.JWEIA.2018.12.016